Hindawi
Wireless Communications and Mobile Computing
Volume 2022, Article ID 2119505, 7 pages
https://doi.org/10.1155/2022/2119505

Research Article

Computer Artificial Intelligence Technology in the Visual Transmission System of Urban Lake Water Quality Inspection and Detection Images

Jian Cui

Male College of Engineering, Inner Mongolia Minzu University, 028000, China

Correspondence should be addressed to Jian Cui; cuijian8309@imun.edu.cn

Received 21 January 2022; Revised 7 March 2022; Accepted 10 March 2022; Published 19 April 2022

Academic Editor: Kalidoss Rajakani

Purpose. Based on artificial intelligence technology, this paper uses the real-time data measured in the monitoring waters and the minimum value of the inversion result map to analyze the logarithmic function relationship. *Methods*. Multitarget tracking algorithm was used to detect lake water quality. A spectral colour difference formula for detecting heavy metal ions in lake water is proposed. *Results*. The research results show that the content of metal ions in water must be detected, and the research method used in this paper is very meaningful. *Conclusion*. The detection method proposed in this paper can improve the detection speed of lake water pollution.

1. Introduction

Metal ion pollution in water is a serious threat. It easily kills animals and plants and threatens human safety. Therefore, we must detect the content of metal ions in water. The existing metal ion detection methods are as follows (Table 1). Existing detection methods have shortcomings [1].

Spectroscopic analysis is an analytical method that uses the principles and experimental methods of spectroscopy to determine substances' structure or chemical composition. Matter emits or absorbs electromagnetic radiation along with electron transitions. Spectral analysis is an analytical method established based on this phenomenon. Various spectral detection methods have been applied to water quality detection in recent years. Fluorescence spectroscopy is an algorithm used alone to estimate the overall pollution status of water quality. UV spectroscopy and fluorescence spectroscopy are combined to measure total carbon, chemical oxygen demand, biochemical oxygen demand, dissolved organic carbon, and permanganate. Spectral remote sensing tests chlorophyll, suspended sediment, oil pollution, and thermal pollution in water. Raman spectroscopy is a method used to detect benzene in water [2]. Because the concentration of metal ions in water responds differently to the visible spectrum, we combine the knowledge of optical chromatic aberration to measure metal ions in water.

2. Experimental Principle

2.1. Visible Spectrum Detection Principle. The visible spectrum is the spectrum that the human eye can perceive. It is visible light between 400 and 760 nm. The visible spectrum is the basis of colorimetry and visible spectrophotometry. Metal ions have the highest absorption for a certain frequency of the spectrum. For example, the absorption wavelength of ferrous ions is 510 mm. The absorption wavelength of copper is 440 nm. Hexavalent chromium has a wavelength of 540 mm. These are in the visible spectral range. The three standard wavelengths of 590 nm, 540 nm, and 438 nm in the existing spectrophotometric calculation methods are also in the range of visible light. Therefore, the visible spectrum meets the detection requirements of metal ions. We describe the spectral properties of colour and establish a three-dimensional spatial coordinate system. We convert spectral features into a single feature, such as chromaticity, Munsell value, and the colour difference between the standard test object.

Table 1: Comparison of existing measurement methods.

Detection method	Advantage	Shortcoming
Atomic absorption	Full measurement parameters and high accuracy	High equipment cost and poor anti-interference
Plasma emission spectrometry	Full measurement parameters and high accuracy	High equipment cost and poor anti-interference
Electrode/spectrophotometry	Fast response and high reliability	Single detection parameter, contact measurement
Ion fluorescence method	Noncontact measurement	Poor universality, few types

Different positions of a metal solution in the three-stimulus value space coordinate can determine the solution concentration. We analyze the spectral properties of a certain concentration of metal solutions under specific illumination. The experiment converts it to a single data colour difference. We obtained the concentration of this metal ion in solution by comparing it with the standard chart.

2.2. CIE Colour Space Theory. A colour space is the description of colours using a colour model. Colorimetry matches all visible colours with red (R), green (G), and blue (B) single-spectral primary colours according to the principle of three primary colours. The three basic colours and hues, brightness and saturation, create different colour spaces. The content includes CMY colour space, HSV colour space, HSI colour space, etc. We use the computer to facilitate the data processing and correction of the colour space based on visual unity. The CIE (International Commission on Luminescence and Illumination) constructed the CIE-XYZ system. The tristimulus space coordinates (X, Y, Z) are expressed as the tristimulus values. We call it the chromaticity value. CIE also specifies two chromaticity spaces: CIE-LUV colour space and CIELAB colour space. The purpose is to represent it on a two-dimensional plane. Both colour spaces are LAB-based colour spaces. We established the visible light colour space with red, green, and blue as the primary colours [3].

2.3. Chromatic Aberration Theory. The International Commission on Illumination has successively proposed three colour difference calculation formulas based on two different colour spaces [4].

(1) The CIE Luv colour difference formula is expressed as follows

$$\begin{cases} L^* = \begin{cases} 116(Y/Y_n)^{1/3} - 16 & (Y/Y_n) > (24/116)^3 \\ 9033(Y/Y_n) & (Y/Y_n) \le (24/116)^3 \end{cases} \\ v^* = 13L^*\left(v' - v'_n\right) \\ u^* = 13L^*\left(u' - u'_n\right) \end{cases} \tag{1}$$

In the Formula, ((1)) is the quantity describing the colour stimulus.u'_n, v'_n represents the colour stimulus value of the selected reference white. The value of u', v' is calculated from formula (2) and formula (3), respectively

$$u' = \frac{4X}{X + 15Y + 3Z} \tag{2}$$

$$v' = \frac{9X}{X + 15Y + 3Z} \tag{3}$$

where X, Y, Z is the tristimulus value of the colour. The formula for calculating the CIELUV colour difference of two-colour samples is as follows

$$\Delta E^*_{uv} = \left[(\Delta L^*)^2 + (\Delta u^*)^2 + (\Delta v^*)^2\right]^{1/2} \tag{4}$$

$\Delta L^* = \Delta L_1{}^* - \Delta L_2{}^* \Delta u^* = \Delta\ u_1{}^* - \Delta u_2{}^* \Delta v^* = \Delta\ v_1{}^* - \Delta v\ {}^*_2$ in formula (4). This represents the difference in colour stimulus for the two samples

(2) The CIELAB colour difference formula and calculation method are as follows

$$\begin{cases} L^* = 116f(Y/Y_n) - 16 \\ a^* = 500[f(X/X_n) - f(Y/Y_n)] \\ b^* = 20[f(Y/Y_n) - f(Z/Z_n)] \end{cases} \tag{5}$$

X, Y, Z in formula (5) represents the tristimulus value of the colour sample. X_n, Y_n, Z_n is the stimulus value of the selected reference white. The function $f(x)$ is expressed as follows

$$f(x) = \begin{cases} x^{1/3} & x > (24/116)^3 \\ \dfrac{841}{108}x + \dfrac{16}{116} & x \le (24/116)^3 \end{cases} \tag{6}$$

This represents the difference in the number of colour stimuli for the two-colour samples

(3) CIEDE2000 colour difference formula is as follows

The CIEDE2000 colour-difference formula is based on the CIELAB colour difference formula. After calculating L^*, a^*, b^*, we continue with the calculation

$$\begin{cases} L' = L^* \\ a' = a^*(1 + G) \\ b' = b^* \end{cases} \tag{7}$$

The calculation formula of G in formula (7) is as follows

$$G = 0.5\left(\sqrt{\frac{\bar{C}_{ab}^{*7}}{\bar{C}_{ab}^{*} + 25^7}}\right) \tag{8}$$

In formula (8), $\bar{C}_{ab}^{*}$ represents the average value of the chroma C_{ab}^{*} of the two-colour samples. See formula (9) for the calculation of chroma C_{ab}^{*}

$$C_{ab}^{*} = \left[(\Delta a^{*})^2 + (\Delta b^{*})^2\right]^{1/2} \tag{9}$$

We calculate C' and h'

$$\begin{aligned} C' &= \left[\left(\Delta a'\right)^2 + \left(\Delta b'\right)^2\right]^{1/2} \\ h' &= \arctan\left(b'/a'\right) \end{aligned} \tag{10}$$

We compute $\Delta L', \Delta C', \Delta H'$ for two-colour samples

$$\begin{aligned} \Delta L' &= \Delta L_1{}' - \Delta L_2{}' \\ \Delta C' &= \Delta C_1{}' \text{-} \Delta C_2{}' \\ \Delta H' &= 2\sqrt{C'_1 - C'_2}\sin\left(\Delta h'/2\right) \end{aligned} \tag{11}$$

where $\Delta h' = \Delta h_1{}' \text{-} \Delta h_2{}'$. Calculate the weighting coefficient S_L, S_C, S_H

$$\begin{aligned} S_L &= 1 + \frac{0.015\left(\bar{L}' - 50\right)}{\sqrt{20 + \left(\bar{L}' \text{-} 50\right)^2}} \\ S_C &= 1 + 0.045\bar{C}' \\ S_H &= 1 + 0.015\bar{C}'T \end{aligned} \tag{12}$$

The formula for T is as follows

$$\begin{aligned} T = 1 &- 0.17\cos\left(\bar{h}' - 30\right) + 0.24\cos\left(2\bar{h}'\right) \\ &+ 0.32\cos\left(3\bar{h}' + 6\right) - 0.20\cos\left(4\bar{h}' - 63\right) \end{aligned} \tag{13}$$

In the above formula, $\bar{L}', \bar{C}'$ and $\bar{h}'$ are the arithmetic mean of the two-colour samples L', C' and h'. The unit of $\bar{h}'$ is degrees the (°). We compute the rotation function

$$\begin{cases} R_T = -\sin(2\Delta\theta)R_C \\ \Delta\theta = 30\exp\left\{-\left[\dfrac{\left(\overline{h'} - 275\right)}{25}\right]^2\right. \\ R_C = 2\sqrt{\dfrac{\bar{C}_{ab}^{*7}}{\bar{C}_{ab}^{*} + 25^7}} \end{cases} \tag{14}$$

The unit of $\Delta\theta$ and $\bar{h}'$ in the formula is (°). We calculate CIEDE2000 colour difference

$$\left(\frac{\Delta L'}{S_L}\right)^2 + \left(\frac{\Delta C'}{S_C}\right)^2 + \left(\frac{\Delta H'}{S_H}\right)^2 + R_T\left(\frac{\Delta C'}{S_C}\right)\left(\frac{\Delta H'}{S_H}\right)^2 \tag{15}$$

CIELAB and CIE2000 are colour difference formulas based on the LAB colour space. The CIELAB chromatic aberration formula errors when calculating some chromatic aberrations [5]. Therefore, the International Commission on Illumination proposed the CIE2000 formula to correct the LAB colour difference formula defects. This paper adopts the CIELUV colour difference formula and CIE2000 colour difference formula for calculation. We compare the two formulas and choose the formula with higher accuracy. The reference object in the experiment is optically pure water

3. Experimental Part

3.1. Reagents and Instruments. The experimental instruments include light source LI38037-W, standard colorimetric lightbox 721 visible spectrophotometers, CCD industrial camera XCG-5005CR, 752N UV-visible spectrophotometer, and bracket OPTES3000-1.

The experimental reagents include acetone, sulfuric acid, phosphoric acid, sodium hydroxide, zinc sulphate, potassium permanganate, potassium dichromate (superior pure), urea, sodium nitrite, and diphenyl carbazide. All the above reagents are of analytical grade unless marked. Solutions were prepared using deionized water [6].

3.2. Experimental Process. We test for hexavalent chromium ions. The experimental process refers to "Water and Wastewater Monitoring and Analysis Method" and the national standard ""Determination of Hexavalent Chromium in Water Quality by Diphenyl carbazide Spectrophotometry." Configure the national standard required concentration samples and pure optical water. We extract images after processing the samples and perform spectrophotometric measurements, respectively. We compare the results of the two methods horizontally and draw a standard concentration curve [7]. Afterward, a random concentration solution was configured for reliability verification. The camera was installed directly above the lightbox before the experiment. This angle makes the incident light perpendicular to the lens. At the same time, the experiment needs to reduce the anisotropy in water. During the experiment, the temperature and humidity of the external environment, the fixed camera aperture, and the focal length were kept as constant as possible.

4. Data Analysis

4.1. Data Processing. We intercept and extract the symmetrical part of the centre of the image and use the visual studio software to call the OpenCV database. The article extracts

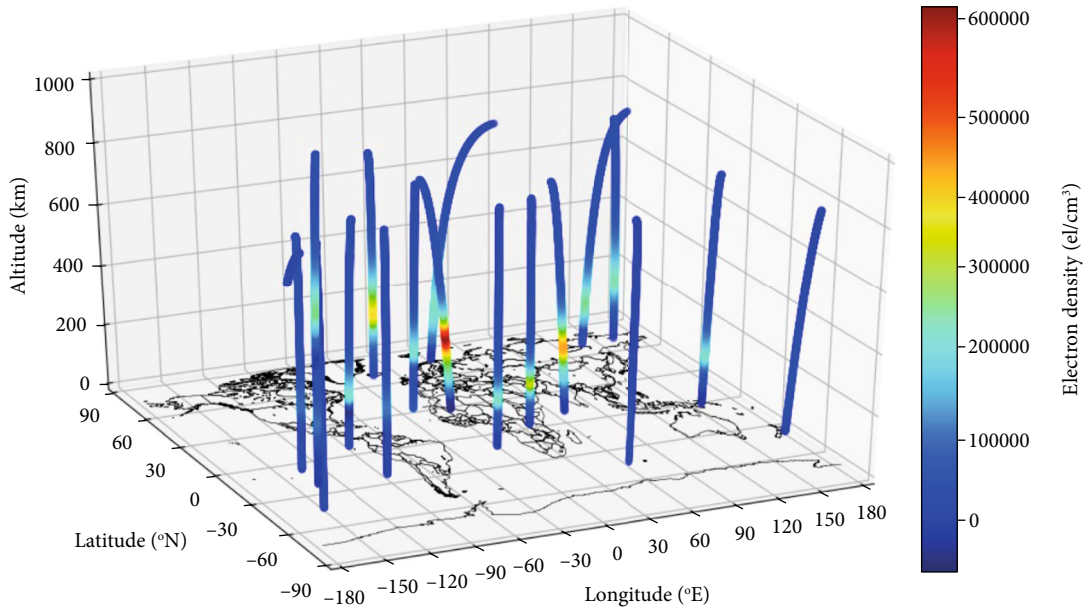

Figure 1: Prefetch consistency.

Table 2: Data extraction rates.

Concentration (mg/L)	0	0.01	0.02	0.05	0.1	0.2	0.5	1
Before data extraction (n)	25507	26169	17126	26693	29231	16111	16637	16634
After data extraction (n)	26972	26572	27602	27223	29727	17111	17141	17351
Extraction rate (%)	94.65	97.45	97.13	97.12	97.65	95.57	97.15	97.37

the R, G, B value of the picture and saves it as the X, Y, Z value. At the same time, we use this as the total amount of data. We examined the consistency of the R-value data at a concentration of 1 mg/L (Figure 1). We can see that some points fluctuate abnormally [8]. Outliers are distributed in bands. The main reasons for the abnormal points are the colour extraction abnormality at the border of the circular image and the singular point at the bottom of the cuvette. Most data can be kept within a narrow range. Since tristimulus values do not vary in isolation, each other is considered when determining the limits. We performed a R, G, B joint filter on the data. The purpose is to avoid data distortion. We separately set the upper and lower limits of R, G, B and remove outliers in the data. The article establishes a normal distribution function and uses $[\mu - 3\sigma, \mu + 3\sigma]$ as the confidence interval. The experiment was to obtain the final data and take the average as the final result. Our final extraction rate is shown in Table 2.

4.2. Data Reliability. The data were normally distributed before extraction. This is in line with statistical laws. The extraction rates of samples with different concentrations were maintained between 94.65% and 98.45%. There are fewer outliers in the image [9]. We use the mean difference and the obtained RGB values when extracting data, as shown in Table 3.

We check for data consistency on postextraction data. It can be seen from Figure 2 that the data volatility is unchanged, and the outliers have been eliminated. It can be seen from Table 3 that the mean difference is small, the data fluctuation value is small, and the reliability is high. The mean difference increases with decreasing concentration. The visible spectrum-colour difference method is unsuitable for measuring very small concentrations [10]. The measurement range is still the range required by the detectable national standard.

Tristimulus value-concentration graphs were drawn from Table 3 (Figure 3). R, G, B is the tristimulus value measured by the colour difference method. R0, G0, B0 are the tristimulus values measured by spectrophotometry. The changes of tristimulus values measured by the two methods were similar. The tristimulus values measured by the colour difference method are largely due to the influence of the light source. When the solution concentration is higher, the tristimulus value of hexavalent chromium is highest in red and lowest in green. When the concentration is low, the variation law of tristimulus value tends to the tristimulus value of pure water.

4.3. Relationship between Metal Ion Concentration and Colour Difference. Table 3 is calculated using the colour difference formulas CIELUV and CIEDE2000. We use the blank solution with a concentration of 0 as the standard to obtain the colour difference. At this point [11], we draw the concentration-colour difference curves separately (Figure 4). The curves obtained by the two different

Table 3: Tristimulus values and mean differences.

Concentration (mg/L)	0	0.01	0.02	0.05	0.1	0.2	0.5	1
R	242.4	214.32	197.42	166.17	137.97	111.66	42.27	34.73
Mean difference	7.11	6.52	6.21	5.42	4.61	4.51	4.47	3.97
G	219.7	164.37	124.95	73.52	46.51	33.95	22.77	17.7
Mean difference	6.21	5.69	5.52	5.23	4.17	1.86	3.1	3.72
B	185.67	175.54	137.91	111.67	78.5	47.93	25.17	21.17
Mean difference	7.14	6.97	6.77	6.63	6.17	3.42	3.23	3.73

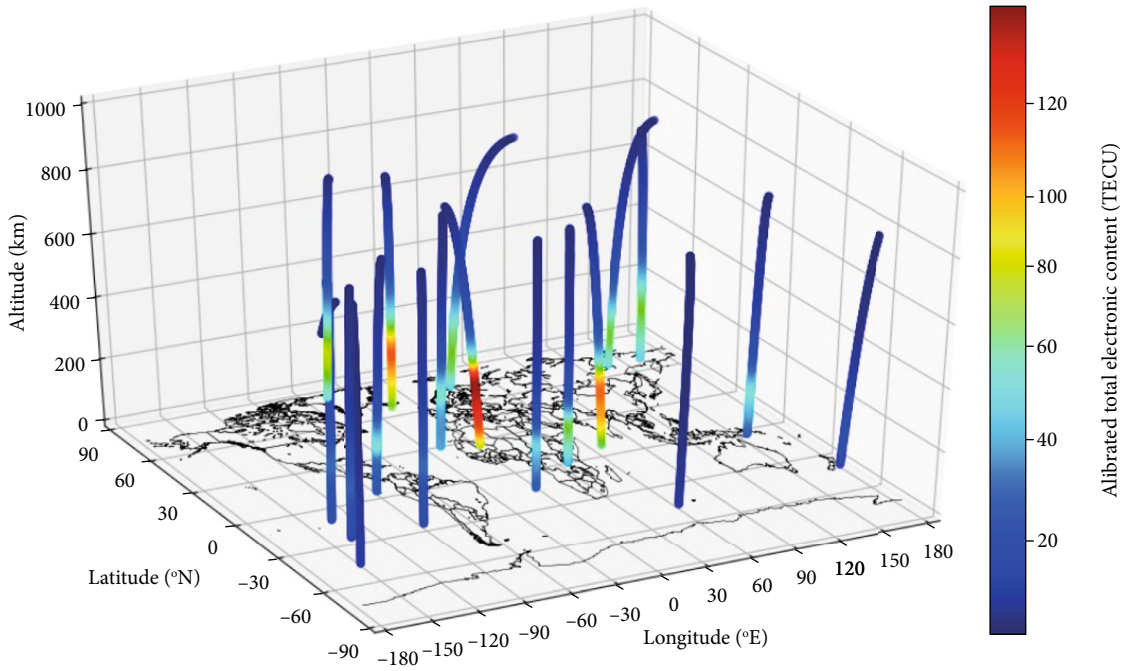

Figure 2: Postextraction consistency.

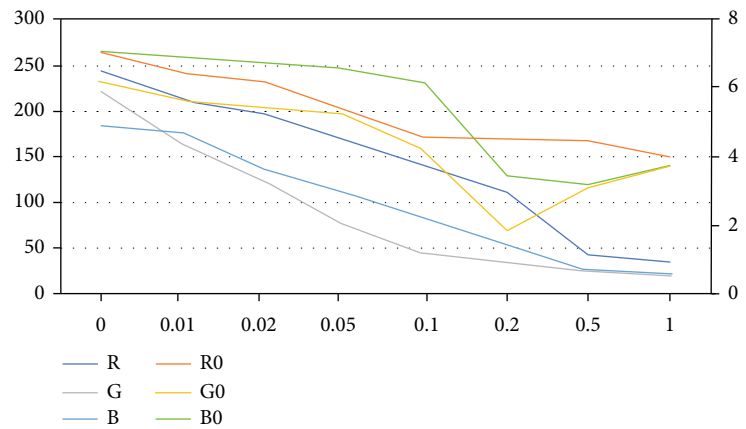

Figure 3: Concentration tristimulus value relationship.

calculations are very similar. They are all logarithmic curves. We fit the data separately. The fitting formula of the colour difference formula CIELUV is $c = 0.000126_e^{0.14488\Delta E_{uv}} + 0.01$. The fitting formula of the colour difference formula CIEDE2000 is $c = 0.000647_e^{0.0214\Delta E_{00}} - 0.00251$. We compare the fitted values with the results obtained by the national standard method, respectively. At this time, the error ranges we get are 1.39%~6.27% and 1.26%~2.92%, respectively. It

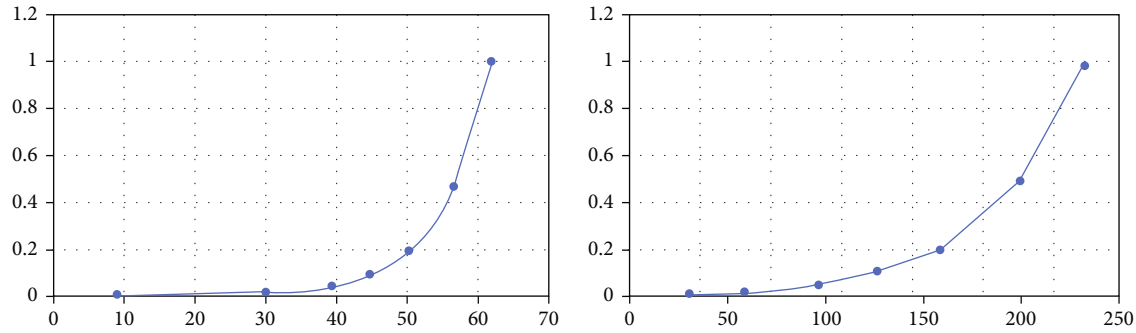

Figure 4: Colour difference fitting diagram.

Table 4: Colour difference fitting accuracy.

Cr6+ concentration (mg/L)	0.01	0.02	0.05	0.1	0.2	0.5	1
△EUV	9.01	29.88	39.38	44.71	50.32	56.58	61.88
Concentration fitting value (mg/L)	0.01	0.02	0.048	0.095	0.195	0.469	0.998
Deviation%	4.659	1.368	4.208	5.438	2.413	6.284	0.301
△E00	30.31	58.24	96.91	126.84	159.69	201.82	234.4
Concentration fitting value (mg/L)	0.01	0.02	0.049	0.098	0.195	0.485	0.988
Deviation%	1.259	2.306	1.885	2.486	2.308	2.918	2.205

can be seen that the DE2000 chromatic aberration method is more accurate. The error is smaller than the national standard for laboratory monitoring requirements. This is far less than the water quality monitoring equipment error requirement ≤3% FS. So, the value meets the national standard. The accuracy of the fitting formula is shown in Table 4 [12].

5. Results

The research results show that the content of metal ions in water must be detected, and the research method used in this paper is very meaningful.

6. Conclusion

Based on the principle of colour difference, this paper analyses point source image data with different concentrations. It draws the following conclusions: (1) The amount of image data collected is large and conforms to normal distribution. The data mean difference is small, and the extraction rate is high. The experimental results show that the data has high reliability. (2) The CCD image acquisition process is completed in the lightbox. In the strong anti-interference ability of the external environment, we can detect metal ion contamination in the visible spectrum. A variety of metal ion detection is effective and used in a wide range of applications. (3) The relative error between the visible spectrum-colour difference method and the national standard method for detecting hexavalent chromium is less than 2.92%. This shows that the method is feasible. The experimental results provide a new idea for remote online detection of multiparameter metal ions in water quality. (4) Different sensitivities of tristimulus values of metal ions under different light sources lead to different chromatic aberrations. Mixed metal ion solutions can be detected using multiple light sources. We plot the curves separately and measure the single metal ion concentration comprehensively.

Data Availability

The data used to support the findings of this study are available from the corresponding author upon request.

Conflicts of Interest

The authors declare no conflicts of interest.

References

[1] X. Wang and W. Yang, "Water quality monitoring and evaluation using remote sensing techniques in China: a systematic review," *Ecosystem Health and Sustainability*, vol. 5, no. 1, pp. 47–56, 2019.

[2] F. Muharemi, D. Logofătu, and F. Leon, "Machine learning approaches for anomaly detection of water quality on a real-world data set," *Journal of Information and Telecommunication*, vol. 3, no. 3, pp. 294–307, 2019.

[3] B. Aghel, A. Rezaei, and M. Mohadesi, "Modeling and prediction of water quality parameters using a hybrid particle swarm optimization–neural fuzzy approach," *International journal of Environmental Science and Technology*, vol. 16, no. 8, pp. 4823–4832, 2019.

[4] A. K. Kadam, V. M. Wagh, A. A. Muley, B. N. Umrikar, and R. N. Sankhua, "Prediction of water quality index using artificial neural network and multiple linear regression modelling approach in Shivganga River basin, India," *Modeling Earth Systems and Environment*, vol. 5, no. 3, pp. 951–962, 2019.

[5] S. Yıldız and C. B. Karakuş, "Estimation of irrigation water quality index with development of an optimum model: a case study," *Environment, Development and Sustainability*, vol. 22, no. 5, pp. 4771–4786, 2020.

[6] L. A. Freeman, D. R. Corbett, A. M. Fitzgerald, D. A. Lemley, A. Quigg, and C. N. Steppe, "Impacts of urbanization and development on estuarine ecosystems and water quality," *Estuaries and Coasts*, vol. 42, no. 7, pp. 1821–1838, 2019.

[7] M. Niroumand-Jadidi, F. Bovolo, and L. Bruzzone, "Novel spectra-derived features for empirical retrieval of water quality parameters: demonstrations for OLI, MSI, and OLCI sensors," *IEEE Transactions on Geoscience and Remote Sensing*, vol. 57, no. 12, pp. 10285–10300, 2019.

[8] A. P. Singh, K. Dhadse, and J. Ahalawat, "Managing water quality of a river using an integrated geographically weighted regression technique with fuzzy decision-making model," *Environmental Monitoring and Assessment*, vol. 191, no. 6, pp. 1–17, 2019.

[9] I. Caballero, R. Fernández, O. M. Escalante, L. Mamán, and G. Navarro, "New capabilities of Sentinel-2A/B satellites combined with in situ data for monitoring small harmful algal blooms in complex coastal waters," *Scientific Reports*, vol. 10, no. 1, pp. 1–14, 2020.

[10] R. H. Becker, M. Sayers, D. Dehm et al., "Unmanned aerial system based spectroradiometer for monitoring harmful algal blooms: a new paradigm in water quality monitoring," *Journal of Great Lakes Research*, vol. 45, no. 3, pp. 444–453, 2019.

[11] D. Antanasijević, V. Pocajt, A. Perić-Grujić, and M. Ristić, "Multilevel split of high-dimensional water quality data using artificial neural networks for the prediction of dissolved oxygen in the Danube River," *Neural Computing and Applications*, vol. 32, no. 8, pp. 3957–3966, 2020.

[12] J. O. Ighalo, A. G. Adeniyi, and G. Marques, "Artificial intelligence for surface water quality monitoring and assessment: a systematic literature analysis," *Modeling Earth Systems and Environment*, vol. 7, no. 2, pp. 669–681, 2021.